JOM
https://doi.org/10.1007/s11837-018-3272-7

SOLID FREEFORM FABRICATION

Microstructural Characteristics, Crack Frequency and Diffusion Kinetics of Functionally Graded Ti-Al Composite Coatings: Effects of Laser Energy Density (LED)

E.O. OLAKANMI,[1,3] M. SEPAKO,[1] J. MORAKE,[1] S.E. HOOSAIN,[2] and S.L. PITYANA[2]

1.—Botswana International University of Science and Technology, Palapye, Botswana. 2.—Laser Enabled Manufacturing Research Group, National Laser Centre/Council for Scientific and Industrial Research, Pretoria, South Africa. 3.—e-mail: olakanmie@biust.ac.bw

This study examines the dependence of microstructural characteristics, crack frequency and diffusion kinetics of functionally graded (FGM) titanium aluminide coatings reinforced with TiC on laser energy density (LED). Samples deposited on a Ti-6Al-4V substrate via single-step laser cladding (LC) were characterised with an optical microscope, scanning electron microscope/energy-dispersive x-ray spectroscopy and x-ray diffraction. LED set at 17.50 J/mm^2 induced a thermo-positive reaction between FGM constituents, which resulted in the formation of intermetallic compounds (e.g., Ti_2AlC, γ and α_2 matrix phases) with a microhardness greater than that of the substrate and least crack frequency. Variation in microhardness across the layers of sample fabricated with 17.50 J/mm^2 is attributed to diffusion kinetics strongly influenced by laser-materials interactions due to the differing chemical composition across its volume. These outcomes provide guidance for a future study that engages the substrate's pre-heat temperature in eliminating microstructural defects via a low-cost and time-effective single-step LC process.

INTRODUCTION

Engineering components made in titanium alloys (e.g. Ti-6Al-4V) are increasingly being employed in the aerospace, automotive and power generation industries because of their excellent high-strength and corrosion-resistance properties. Nevertheless, the utilisation of Ti-6Al-4V in these industries has been restricted by its limited working temperature, which is $< 400°C$, as well as poor wear resistance.[1] Hence, there is a need to employ an appropriate surface modification technique to address these challenges associated with the functional performance of Ti-6Al-4V in the industries. Surface modification technology entails the deposition of a material having superior functional performance on another material with less desirable functionalities. The goal is to improve the performance of a material having less than desirable functionalities. It has been implemented via laser cladding (LC),[2,3] high-velocity oxy-fuel (HVOF) and plasma spraying (PS).[4] Compared with all the listed surface modification technologies, LC imparts the strongest metallurgical bonding when engaged in improving the functional performance of engineering parts.

Extending the working temperature of Ti-6Al-4V as well as improving its wear resistance requires designing new materials with superior functional performance. Functionally graded materials (FGM) possess the capabilities to extend the service of Ti-6Al-4V in a working environment. FGMs have varying microstructural, mechanical and physical properties because of the gradual modification in chemical composition over its entire volume.[5,6] The constituent dissimilar materials in FGMs compensate for each other's weaknesses with a view to developing a product with enhanced functional performance compared with each of the parent materials when deposited singly. These account for the increasing popularity of FGMs in various industrial sectors as demonstrated by Nazarov et al.[7] who developed an FGM nickel aluminide (Ni-Al) system

Published online: 07 December 2018

for aviation application. The titanium aluminide (Ti-Al) coating is an FGM system that is gaining industrial and academic attention because of its excellent elastic modulus, specific strength, creep strength and excellent temperature oxidation resistance.[8,9] Meanwhile, the Ti-Al coating is characterised by undesirable room temperature ductility, susceptibility to cracking and poor wear resistance.[10] Controlled dispersion of reinforced particulates into an FGM titanium aluminide matrix could be engaged to improve its undesirable wear characteristics as this has been reported to enhance its wear resistance as well as associated microstructural and mechanical properties.[2] Furthermore, pre-heating of the substrate has also been employed to eliminate the crack susceptibility of an FGM composite Ti-Al system. In an attempt to increase the range of service temperatures at which parts made in Ti-6Al-4V can be utilised as well as improve its wear resistance in the automotive, aerospace and power-generation industries, this study employs LC combined with pre-heating in depositing a Ti-Al reinforced particulate FGM composite on a Ti-6Al-4V substrate.

Literature on LC-fabricated FGM-reinforced particulate composites is scarce.[2] For instance, Abboud et al.[2] explored the effects of the scan velocity, powder feed rates and number of layers on the geometrical characteristics, microstructural variation and wear properties of Ti-Al/TiB_2 FGM composites. The study revealed that samples were porous and characterised by cracks. To establish a basis for manufacturing FGM parts for extending the high temperature service life and wear resistance of Ti-6Al-4V components in the automotive, aerospace and power-generation industries, this study examines the effects of laser energy density (LED) on the microstructural characteristics, crack frequency and diffusion kinetics of Ti-Al/TiC FGM composites fabricated with a single-step LC process at a constant preheating temperature of 400°C. LED combines the influence of laser power (P), scanning velocity (V) and beam diameter (d) to understand the role of laser-materials interaction in the microstructural evolution, crack frequency and diffusion kinetics of the composite coatings. To understand the diffusion kinetics underlying the formation of the coatings, the effects of chemical composition on the laser-materials interactions across the FGM were explored.

MATERIALS AND METHODOLOGY

Materials

Commercially available elemental gas atomised aluminium (Al: 45–90 μm), grade 1 titanium (Ti: 45–90 μm) and irregularly shaped titanium carbide (TiC: 45–90 μm) morphology were employed to fabricate the FGM composite. The purity of Ti, Al and TiC powders was 99.9%. The powders were supplied by TLS Technik GmbH. The feed rate in g/min of each powder was determined via the flowability graphs. The component ratio of the FGM composite constituents was determined by using the ratio of the feed rate of the parent materials. A titanium aluminide (Ti-Al) system consisting of 50 wt.% Ti-50 wt.% Al was formulated initially, and the morphologies of the blended powders and that of TiC are shown in Fig. 1a and b respectively. A Ti-Al/TiC FGM composite coating was developed by varying the component ratio starting with 0 wt.% TiC/100 wt.% Ti-Al in increments of 10 wt.% up to 40 wt.% TiC/60 wt.% Ti-Al. Composition across each of the five layers of the volume of the FGM was varied according to the component ratio.

Methodology

Prior to deposition, Ti-6Al-4V substrates with dimensions of 100 mm × 100 mm × 5 mm were cleaned with acetone to remove impurities from their surfaces and enhance the quality of the laser clad. Laser power (1.25 kW, 1.50 kW and 1.75 kW) was varied, while the scan speed (V = 25 mm/s), spot diameter (d = 4 mm), stand-off distance (12.00 mm), shielding gas flow rates (10.00 L/min), carrier gas flow rate (2.00 L/min) and substrate's pre-heat temperature (400°C) were fixed. Laser energy density (LED) in J/mm^2 is defined as shown in Eq. 1:

$$\mathrm{LED} = {}^{P}/_{V * d} \tag{1}$$

The deposition of the FGM particulate-reinforced composite in single-track and multi-layers was achieved via a 3-kW IPG continuous fibre laser system. Then, FGM constituent materials were injected into the melt pool on a substrate pre-heated at 400°C. A three-way coaxial nozzle system connected to a five-axis CNC machine and a 1.5-bar GTV multi-hopper powder feed system was used for powder feeding. The powder feed system regulates the powder feed rate through its rotary speed. The flowability graphs of the powders were used to determine the component ratio of the FGM constituent materials. The shielding and carrier gases used in the experimental work are both made of argon gas. Samples produced were replicated twice.

Sample Analysis

Cross sections of the deposited FGM clad samples were obtained at the middle of the track for microstructural and compositional characterisation. Thereafter, the sectioned FGM clads were ground and polished to a 0.04-μm (OP-S suspension) surface finish with a Struers TegraForce-5 auto/manual polisher. The samples were etched in Keller's reagent for 2–3 min so that the microstructural characteristics were determined by an Olympus optical microscope equipped with Analysis® software. A Jeol JSM-7100F scanning electron

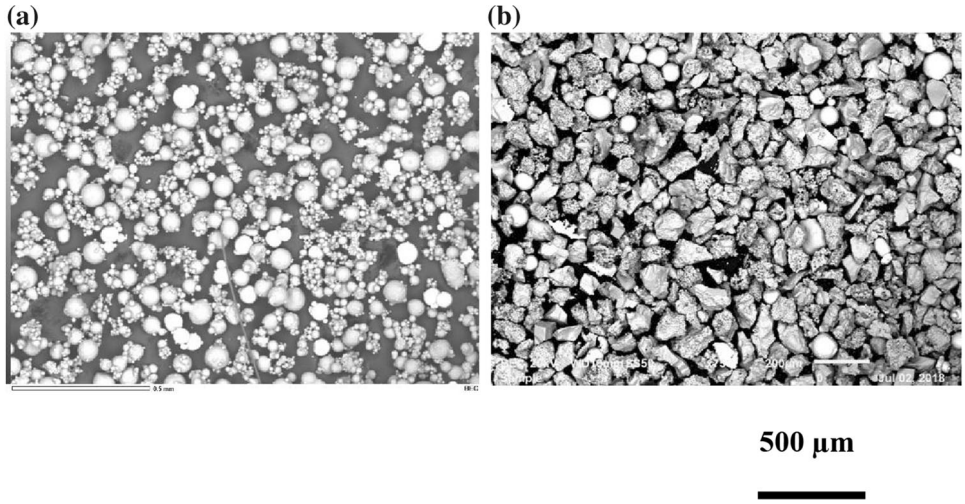

Fig. 1. Scanning electron micrographs showing the surface morphologies of the powders used in this study. (a) Titanium aluminide (Ti-Al); (b) titanium carbide (TiC).

microscope (SEM) equipped with energy-dispersive x-ray spectroscopy (EDS) was used to carry out the microstructural and elemental analysis of the FGM composites as well as examination of its crack surfaces. Crack frequency (CF) was calculated according to Eq. 2 where N is the number of cracks counted in the vertical cross section of the observed deposits, A is the area of clad in (mm^2) and L is the length of the clad deposit.

$$CF = {}^{(N \times L)}/_{(A)} \quad (2)$$

The phase composition of the FGM composite clads was identified via x-ray diffraction (Model Bruker D8 Advance) with a Cu Kα radiation source. Material PDF files were used to identify the phases present in the FGM composite coatings. Microhardness values of the FGM composite coatings were determined using a model MHT-1 Matsuzawa Seiko Vickers microhardness tester. The indenting load used was 500 g with a dwell time of 10 s for each indentation. Microhardness measurements were taken along the length of the coating at 100-μm spacing as well as the interface between the substrate and FGM composite coating. The experimental findings reported in this study were the average values of the corresponding results of the two groups of experiments.

RESULTS AND DISCUSSION

Effects of Energy Density on Microstructural Evolution in Laser-Fabricated FGM Composite Clads

Figure 2a–i provides insight into how variation in LED alters the microstructure of the FGM across its volume. Figure 2 shows that irrespective of the amount of LED dissipated in fabricating the FGM, the particle size of unmelted TiC diminishes in varying degrees relative to the particle size (45–90 μm) of the starting powder (Fig. 1b). This suggests that TiC particles melted and dissolved in the melt pool. Furthermore, independent of the LED, the sizes of unmelted TiC particles in the samples grow increasingly as follows: top layer $\rightarrow$ middle layer $\rightarrow$ bottom layer. Thus, increased consolidation occurred at the lower section compared with the top section of the FGM. The growth in the size of unmelted TiC particles as well as increased consolidation from the top to lower layer of the FGM composite samples is elucidated by the phenomenon of directional solidification in which heat is dissipated away from the top to bottom layer.[11]

Figure 2a–c, d–f and g–i shows the microstructure of the FGM composite fabricated with 12.50 J/mm^2, 15.00 J/mm^2 and 17.50 J/mm^2 respectively. It is clear that the amount of TiC melting and dissolving in the FGM melt pool varies as the LED with sizes of unmelted TiC particles reducing as follows: 12.50 J/mm^2 $\rightarrow$ 15.00 J/mm^2 $\rightarrow$ 17.50 J/mm^2. The sample made with LED of 17.50 J/mm^2 (Fig. 2g–i) is distinguished from those fabricated with 12.50 J/mm^2 (Fig. 2a–c) and 15.00 J/mm^2 (Fig. 2d–f) as its microstructure is characterised by unmelted TiC particles as well as fine dendrite and needle-like phases at all locations across the volume of the FGM. In addition, dendrites are finest at the top layer compared with the middle and lower layers. Figure 3 shows the microhardness ($HV_{0.5}$) across the layers of FGM composite clad samples at varying LEDs from the top surface of the deposits to the substrate. The microhardness of the FGM composite clads is presented with standard deviation of $\pm$ 10%. Figure 3a clearly shows that the microhardness across the layers was constant ($\sim$ 100 $HV_{0.5}$) and significantly less than that of the substrate. This outcome is not surprising as the applied LED of 12.50 J/mm^2 does not effectively initiate metallurgical reactions among Ti, Al and C to ensure formation of inter-metallics, which could have imparted higher microhardness across the

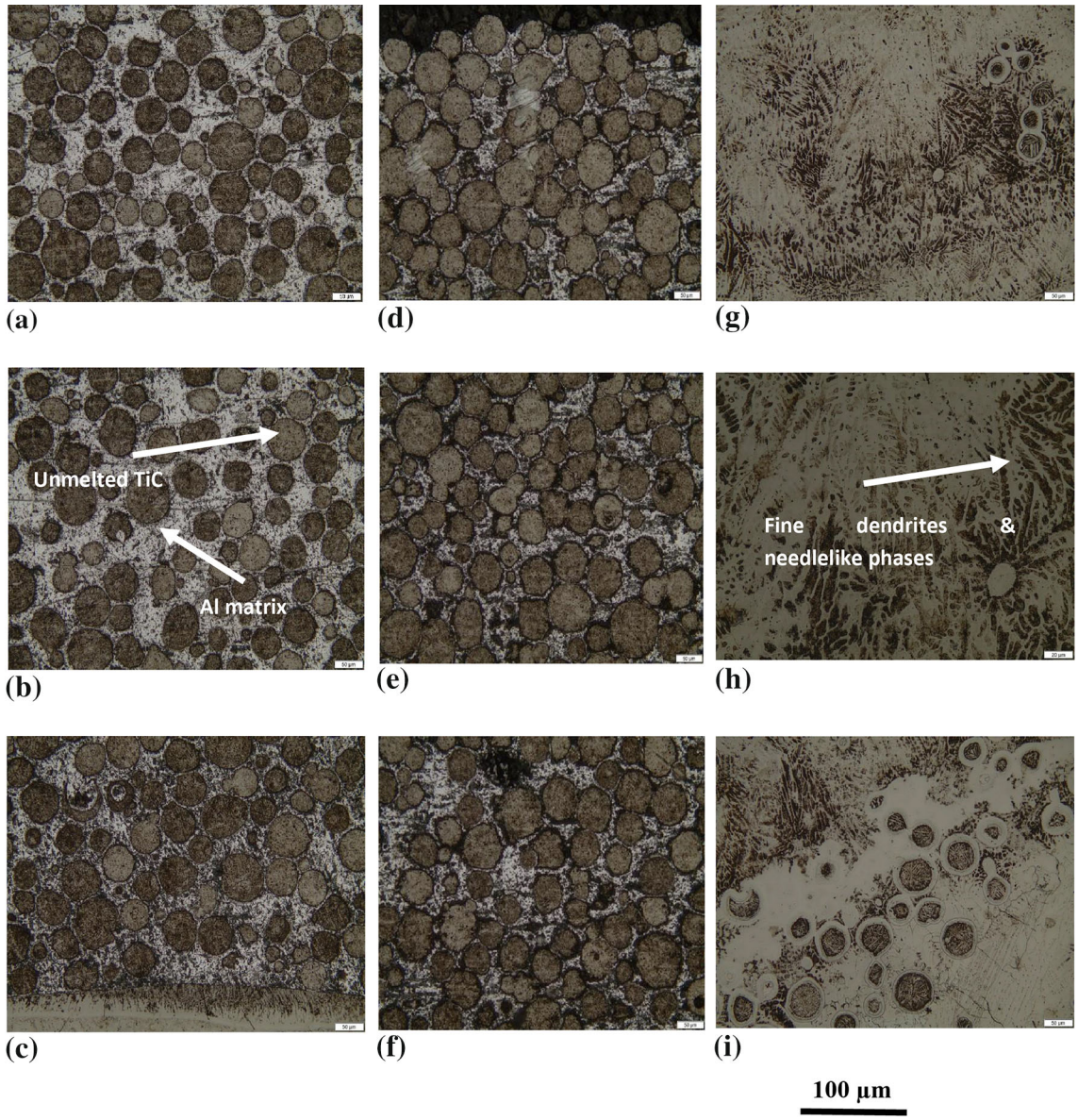

Fig. 2. Optical micrographs of the FGM composite fabricated with 12.5 (a–c), 15.0 (d–f) and 17.5 J/mm^2 (g–i) viewed at the top layer (a, d, g), middle layer (b, e, g) and lower layer (c, f and i).

FGM layers. A marginal increase in microhardness across the FGM layers is noted for samples deposited with LED of 15.00 J/mm^2 relative to that of 12.50 J/mm^2. The microhardness across the layers is however less than that of the substrate. Similar to the sample deposited with 12.50 J/mm^2, there is no difference in the microhardness across the second to fifth layers except in the first layer in which the microhardness is $\sim$ 200 $HV_{0.5}$. This indicates that the adopted process parameter is just sufficient to initiate gradient composition in the first layer alone. With LED increasing to 17.50 J/mm^2, the microhardness profile (Fig. 3c) obtained across the FGM composite clad layers compares favourably to the two-layer FGM Ti-Al/TiB_2 composite.[2] Except for the first layer, the microhardness across the last four layers is either equal to or higher than that of the substrate (Fig. 3c). Meanwhile, a variation in microhardness across the layers of the sample fabricated with LED of 17.50 J/mm^2 is observed. This could be attributed to the influence of different laser-materials interactions accounted for by differing chemical compositions across the FGM volume.

The nature of laser-materials interaction guiding the LC processing of FGM composite is incomplete metallurgical melting.[3] In incomplete metallurgical melting, the higher melting point reinforcing the TiC structural phase encounters partial melting whereas the Ti-Al matrix is completely liquefied. Meanwhile, the viscosity of the melt pool is excessively high upon the introduction of 100% Ti-Al into first layer during LC processing as it encounters full

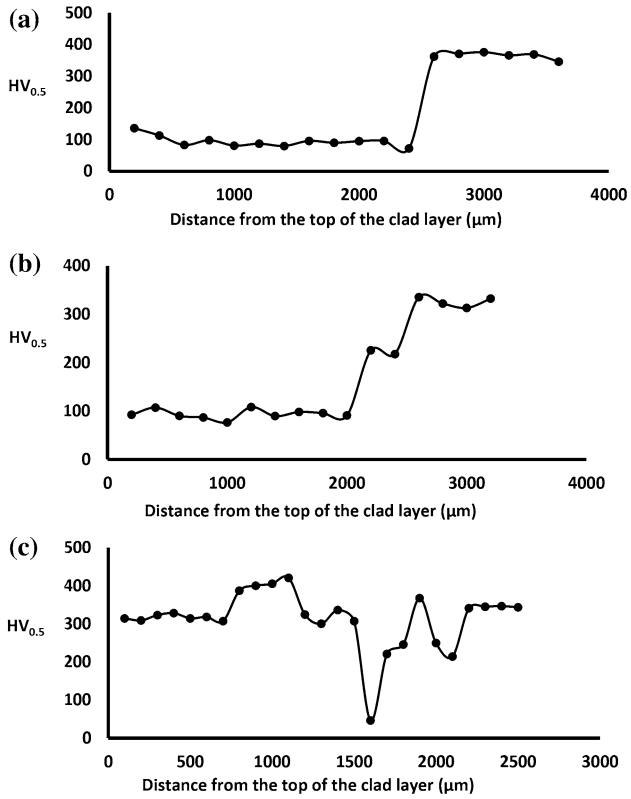

Fig. 3. Microhardnesses ($HV_{0.5}$) across the layers of FGM composite clad samples at varying LEDs from the top surface of the deposits to the substrate: (a) 12.50 J/mm^2, (b) 15.00 J/mm^2 and (c) 17.50 J/mm^2.

melting. A highly viscous molten pool is not able to flow efficiently; hence, it is characterised by diminishing rheological behaviour. According to Olakanmi et al.,[3] the development of intensive Marangoni convection within the molten pool at the first layer introduces an additional force into the pool such that it flows radially towards the centre of the laser beam in preference to spreading outward on the underlying surface. This behaviour of the first layer melt pool could be attributed to the combined influence of the rheological characteristics of the melt being diminished by its excessively high viscosity as well as the Marangoni force. Consequently, the melt pool in the first layer takes longer than necessary to solidify; hence, this has an adverse effect on the densification of this layer as evident in the occurrence of micro-porosities, which reduces the microhardness of the first layer (Fig. 3-c). The microhardness across the FGM volume increases as the TiC content increases consequent to its partial melting. Therefore, the melt pool in the second, third, fourth and fifth layers is not superheated because of partial melting of Ti-C, which does not allow for excessive in situ chemical reactivity between the Ti-Al and TiC particles. In situ chemical reactivity introduces additional thermal energy during laser-materials interaction. In the layers above the first layer, it can be inferred that the rheological properties of the melt pool were not impeded by excessive melt viscosity and the effect of the Marangoni force. Across these layers, the solidification of the melt pool occurs within an adequate time anticipated for the formation of an improved microstructure characterised by enhanced microhardness (Fig. 3c). Therefore, the impartation of microhardness values higher than that of the substrate at the last four layers of this sample points to (1) the Ti-Al matrix alloying with aluminium as well as the partial melting of TiC, which results in the precipitation of primary TiC crystals, and (2) refinement of the microstructure at these layers upon the occurrence of the phenomenon of rapid solidification.

Meanwhile, reduced microhardness reported for the sample at the first layer and interface could be attributed to the undesirable influence of the directional solidification in which excessive heat being transferred from the top layers to the first layers and the interface might have induced microstructural defects at the first layer and interface.

Effect of Laser Energy Density on Crack Frequency in the Laser-Fabricated FGM Composite

Analysis of SEM micrographs for the samples indicates that a clad is characterised by a smaller cross-sectional area and more cracks at low LED compared with high LED. Therefore, the data for clad area (A) and the number of cracks (N) generated for the 40 mm (L) deposit at varying LEDs were employed to calculate the crack frequency (CF) via Eq. 2. The CF of the FGM composite clads is presented with ± 5% standard deviation. Figure 4a clearly shows that the crack frequency (number of cracks per unit length of deposits) varies inversely with the LED. This is elucidated by the solidification phenomenon of the LC process, which is a function of LED. Considering a point heat source travelling in a semi-infinite medium, Eq. 3, formulated according to the three-dimensional (3-D) Rosenthal solution,[12] suggests that the cooling rate $\left(\partial T/\partial t\right)$ increases as the incident LED $\left(P/V*d\right)$ reduces where k is the materials' thermal conductivity and T_0 is the temperature of the substrate.

$$(\partial T/\partial t) \propto \left(\left(k(T-T_0)^2\right)\Big/(P/V*d)\right) \qquad (3)$$

A diminished tendency in the occurrence of cracking at higher incident LED is accounted for by the resultant lower cooling rates. In concurrence with Patterson et al.[13] and Liu and DuPont,[14] the susceptibility of the FGM composite to cracking at lower laser energy density is due to induced thermal stresses in its constituent materials that exceed its fracture strength upon solidification within a temperature range for which ductility was minimised. Therefore, the Ti-Al composite FGM is prone to

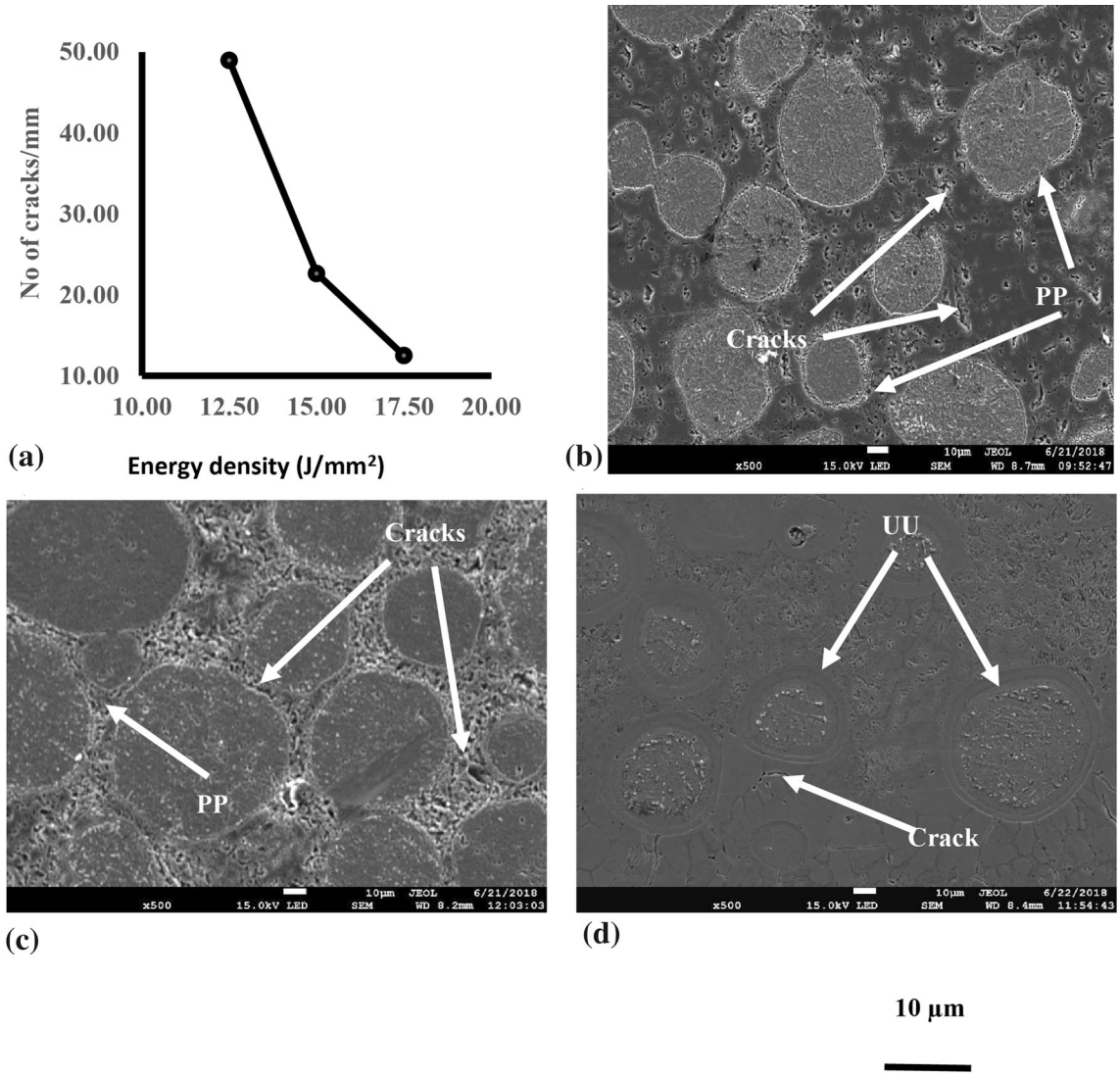

Fig. 4. (a) Relationship between cracking frequency and LED. (b) Scanning electron micrographs (SEM) showing the nature as well as mechanism of crack propagation in the LC-fabricated Ti-Al composite FGM coating: (b) 12.5 J/mm^2, (c) 15.0 J/mm^2 and (d) 17.5 J/mm^2.

cracking during LC processing. Although all the samples were pre-heated at 400°C, cracking still occurred in the coatings irrespective of the LED adopted to fabricate the FGM coatings. This implies that alteration of the LC process parameters alone cannot achieve the fabrication of a crack-free Ti-Al composite FGM coating. Hence, future study will consider how variation in the substrate's pre-heat temperature in synergy with LC process parameters engineers a defect-free microstructure and enhanced functional performance of the FGM composite coating.

The nature as well as mechanism of crack propagation in the LC-fabricated Ti-Al composite FGM coating is presented in Fig. 4b–d as a function of LED. Cracks originating from the boundary of unmelted TiC particles due to poor bonding (see region PP in Fig. 4b and c) between the unmelted Ti-C particle and solidified Ti-Al matrix are associated with samples fabricated with 12.5 J/mm^2 and 15.00 J/mm^2. Similar to the outcome from Chen,[15] the grain structure in the unmelted particles of these samples is not fully developed; hence, the core of the as-received powders remained as unmelted particles because of insufficient laser energy density (12.5 J/mm^2 and 15.00 J/mm^2) being dissipated for LC processing. Consequently, a semi-continuous brittle film existing at the boundaries of the unmelted particle in addition to the poor bonding resulting from poor wettability at the Ti-Al matrix/TiC particle boundaries accounts for cracking along the unmelted particle boundaries under thermal stress in samples fabricated with energy density of 12.5 J/mm^2 and 15.00 J/mm^2. In Fig. 4d, no crack is observed to have propagated from the boundary of partially melted TiC particles. Compared with Fig. 4b and c, a stronger bonding (see region UU in Fig. 4d) exists between the

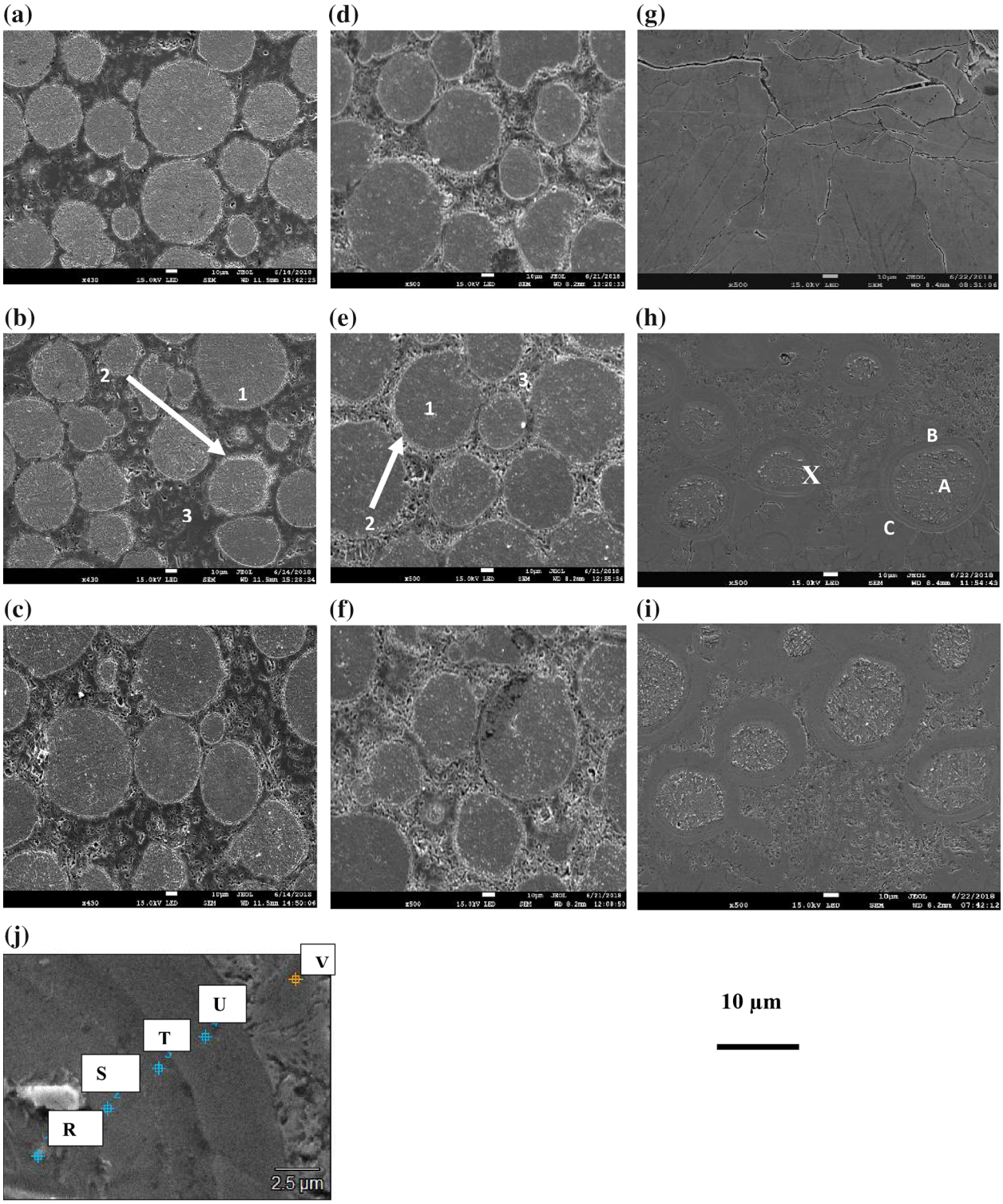

Fig. 5. Scanning electron micrographs (SEM) of the FGM composite fabricated with 12.5 (a–c), 15.0 (d–f) and 17.5 J/mm^2 (g–i) viewed at the top layer (a, d, g), middle layer (b, e, g) and lower layer (c, f and i); (j) observation of regions A, B and C in h at higher magnification.

partially melted Ti-C particle and solidified Ti-Al matrix when samples are fabricated with 17.5 J/mm^2. This could be ascribed to the formation of a well-developed grain structure of the partially melted TiC particles due to sufficient LED (17.5 J/mm^2) being dissipated for LC processing. As a result, the sufficient LED disrupts the semi-continuous brittle film existing at the boundaries of the TiC, thereby paving the way for the dissolution of carbide into the FGM melt pool. This effectively

Table I. Typical chemical composition of FGM samples fabricated with varying LEDs as obtained by EDS and XRD analysis showing the phases present

Table no.	Samples	Regions	Chemical composition C	Al	Ti
EDS analysis					
a	12.0 J/mm^2 and 15.0 J/mm^2. (Fig. 5a–c, d–f)	1	0.87		99.13
		2	8.33	85.68	5.98
		3	5.17	94.19	0.64
b	17.5 J/mm^2 (Fig. 5h) regions A, B and C	R	0.80		99.20
		S	0.92	0.97	98.11
		T	1.74	11.65	86.60
		U	2.12	20.88	77.00
		V	2.60	37.56	59.84

Table no.	Phase	2 Theta angles	Phase composition 12.50 J/mm^2	15.00 J/mm^2	17.50 J/mm^2
XRD analysis					
c	A: γ-TiAl	21.92, 38.95, 44.73, 78.57	√	√	√
	B: α_2-Ti_3Al	35.65, 40.90, 53.81, 64.64, 77.96	√	√	√
	C: TiC	35.65, 40.90, 53.81, 76.92	√	√	√
	D: Ti_2AlC	40.91, 53.91	√	√	√
	E: Ti	35.75, 36, 06, 40, 50, 53, 60, 55, 46, 71, 25			√

prevents the propagation of cracks along the Ti-Al matrix/TiC particle boundaries. Meanwhile, it is observed in all the samples that crack also originate from the interface between the deposit and substrate such that the crack plane is perpendicular to the substrate.

Diffusional Kinetics Laser-Cladded FGM Composite Coatings

Scanning electron micrographs (SEM) of the samples deposited with LEDs of 12.50 J/mm^2, 15.00 J/mm^2 and 17.50 J/mm^2 are shown in Fig. 5a–c, d–f and g–i respectively with a view to elucidating the diffusional kinetics guiding its microstructural evolution and cracking efficiency. The microstructures of coatings fabricated with 12.50 (Fig. 5a–c) and 5.00 J/mm^2 (Fig. 5d–f) both consist of grey-coloured unmelted TiC particles (1), a white-coloured ring region surrounding the unmelted TiC particle (2) and a dark-coloured region (3).

Comparative analysis of the samples fabricated with 12.50 J/mm^2 (Fig. 5a–c) and 15.00 J/mm^2 (Fig. 5d–f) reveals that the thicknesses of the white-coloured ring regions (2) are larger in the latter. The thickness of these white-coloured ring regions is also noted to be increasing from the top to lower layers of the FGM samples irrespective of the LED employed for deposition. Meanwhile, the widths of regions 1 and 3 have decreased in samples fabricated with 15.00 J/mm^2 (Fig. 3d–f) relative to those with 12.50 J/mm^2. EDS analysis was implemented to determine the chemical composition of regions 1, 2 and 3 formed in FGM samples fabricated with 12.50 J/mm^2 and 15.0 J/mm^2 (Fig. 5a–c and d–f). Table Ia confirms that the grey-coloured region 1 is rich in titanium with a trace quantity of carbon; the white-coloured ring region 2 consists of aluminium, carbon and titanium, while the dark-coloured region 3 consists of aluminium and carbon with a trace quantity of titanium. The formation of white-coloured ring region 2 indicates the occurrence of a metallurgical reaction among aluminium, titanium and carbon, while the existence of region 3 indicates there was diffusion of carbon to the aluminium-rich dark areas.

Figure 5g–i reveals the evolution of distinct microstructural features for samples deposited with 17.5 J/mm^2. For instance, three regions consisting of the core (A) surrounded by layers (B) and sandwiched between region C are shown in Fig. 5h. The area marked *X* in Fig. 5h is a representative area consisting of A, B and C, which is observed at higher magnification (Fig. 5j). Figure 5j reveals that the core region R is surrounded by layers S, T and U with the layers sandwiched in the lighter grey region V. The EDS analysis of the regions is shown in Table Ib. Analysis of Fig. 5j and Table Ib confirm that an in situ reaction synthesis occurred between the Ti-Al and TiC powders when LED of 17.5 J/mm^2 was dissipated for processing as the isolated titanium-rich (*R*) and aluminium-rich (*T*) regions, which are associated with FGM composites fabricated with lower LED (Fig. 5a–c and d–f), have decreased in size (Fig. 5g–i). This occurred as

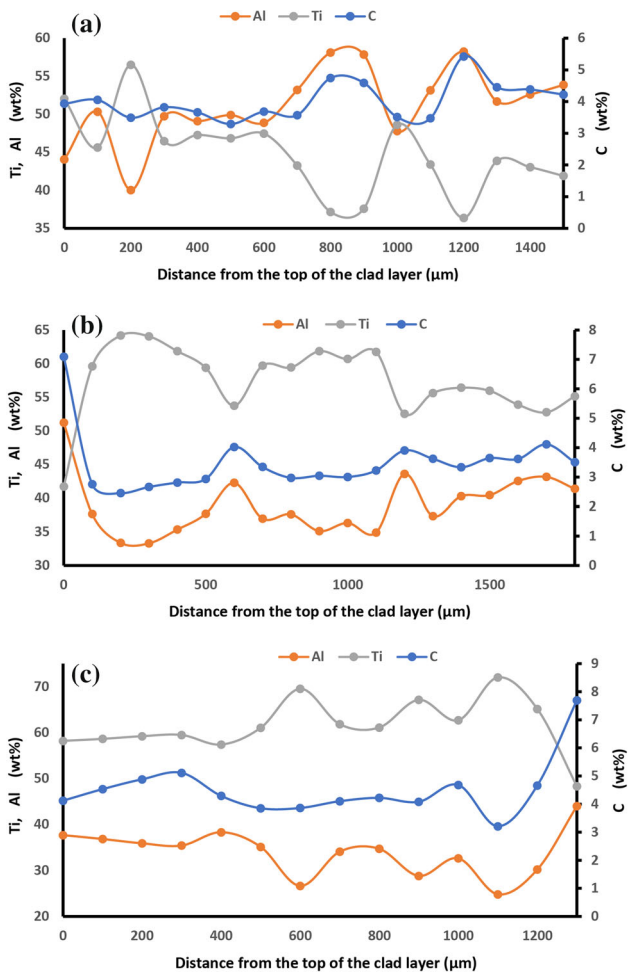

Fig. 6. EDS point test data for the composition curves of FGM composite fabricated with (a) 12.50 J/mm^2, (b) 15.00 J/mm^2 and (c) 17.50 J/mm^2.

aluminium and carbon atoms diffused inward into the titanium core.

Figure 6a–c depicts the EDS point test data for the composition curves of the FGM composite fabricated with 12.50 J/mm^2, 15.00 J/mm^2 and 17.50 J/mm^2 respectively. The EDS point test data are presented with ± 10% standard deviation. Figure 6 shows that the EDS of all FGM composite clads possesses the following features in common: immediate lift and dip as well as up and down stagger irrespective of the LED employed during fabrication. Meanwhile, intersection is only evident across the length of the sample fabricated with 12.50 J/mm^2 (Fig. 6a) and at the top layer of the FGM composite clad deposited with 15.00 J/mm^2 (Fig. 6b). The occurrence of these features on the compositional curves suggests the trends in the elemental concentration across the volume of the FGM composite.

Figure 6a–c shows that at instances when titanium diffuses faster, both aluminium and carbon tend to diffuse very slowly and vice versa. At 12.50 J/mm^2, it is established that Ti atoms diffuse more slowly than aluminium and carbon atoms (Fig. 6a). As the LED increases to 15.00 J/mm^2 and 17.50 J/mm^2, titanium atoms diffuse faster than aluminium and carbon atoms (Fig. 6b and c). With LED set at 12.50 J/mm^2, the concentrations of diffused aluminium atoms are above the expected values of 50 wt.%, 45 wt.%, 40 wt.%, 35 wt.% and 30 wt.% for each of the first, second, third, fourth and fifth layers respectively, whereas the concentrations of dissolved titanium atoms across at all the layers are below the expected values. This could be because the dissipated LED is only effective at melting many of the aluminium atoms to the detriment of titanium atoms. Meanwhile, at LEDs of 15.00 J/mm^2 and 17.50 J/mm^2, the concentrations of aluminium atoms are well below the expected values across the layers while those of titanium are well above the expected concentration values across the layers. Notably, the concentrations of dissolved titanium atoms across the layers of the FGM composite clad fabricated with 17.50 J/mm^2 are higher than those of 15.00 J/mm^2 while the converse is true for aluminium.

The concentration of diffused carbon atoms across layers is constant at values varying between 3.00 wt.% and 4.00 wt.% for samples fabricated with 15.00 J/mm^2 and 17.50 J/mm^2. The concentration of diffused carbon atoms across FGM layers at 15.00 J/mm^2 and 17.50 J/mm^2 is lower than that of 12.50 J/mm^2. The reduced concentration of aluminium below the expected values across the layers at 15.00 J/mm^2 and 17.50 J/mm^2 indicate that aluminium atoms might have evaporated as the specified LED might have induced a processing temperature higher than the melting point of aluminium. An increased concentration of titanium atoms for samples deposited with 15.00 J/mm^2 and 17.50 J/mm^2 suggests an increasing trend in the formation of intermetallic compounds among Ti, Al and C atoms. Meanwhile, it is anticipated that the phase composition of intermetallic compounds forming from metallurgical reactions among Ti, Al and C atoms will increase in the following order: 12.50 J/mm^2 → 15.00 J/mm^2 → 17.50 J/mm^2.

XRD analysis (Fig. 7a and Table Ic) of the samples confirms the formation of Ti_2AlC (titanium aluminide carbide) in the FGM composites in addition to γ and α_2 matrix phases while some TiC phases are still retained within the microstructure. The presence of TiC phases in the microstructure affirms that TiC particles were partially melted. The relative intensity of diffractive peaks (Fig. 7a) for α_2 in the FGM composite clads is significantly enhanced as LED increases.

This emphasises that the increase in the volume fraction of the α_2 matrix occurs as LED increases. Findings reported in Figs. 5a–i, 6 as well as Table Ia and b support this claim that the propensity of metallurgical reactions involving Ti and Al tends to increase as LED increases. According to Liu and DuPont,[14] for a melt pool containing > 2 at.% carbon at processing temperatures > 2200°C, primary TiC_{1-}

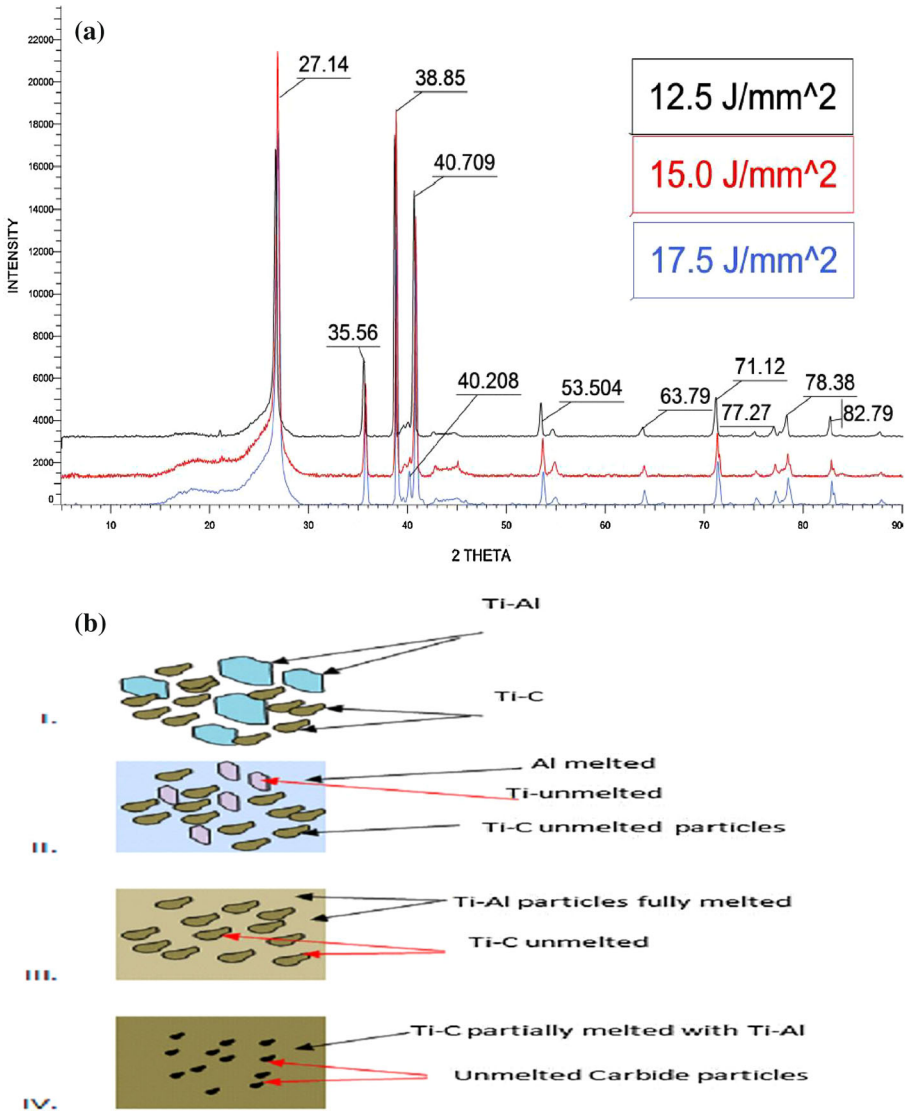

Fig. 7. (a) XRD analysis of FGM composite clad samples fabricated with LED of 12.50, 15.00 and 17.50 J/mm^2; (b) TiC/TiAl diffusion kinetics.

$_x$ initially solidifies. Thereafter, a peritectic reaction in which $TiC_{1-x} + L \rightarrow Ti_2AlC$ occurs as the melt pool cools down to 2200°C. Further cooling of the melt pool below 2200°C leads to the precipitation of the ternary Ti_2AlC because of depletion of the carbon content in the liquid composition. Later, in a different peritectic reaction $L + Ti_2AlC \rightarrow \beta$-Ti(Al) occurs. Liu and DuPont[14] also reported that the reaction $L + \beta \rightarrow \alpha + Ti_2AlC$ could occur at the final stage of LC processing. Given the available information from the work of Liu and DuPont,[14] the phase transformation scheme for the FGM composite clads is elucidated as follows:

$$L \rightarrow TiC + L \rightarrow TiC + Ti_2AlC + L \rightarrow TiC + Ti_2AlC + \beta + L \rightarrow TiC + Ti_2AlC + \alpha \rightarrow TiC + Ti_2AlC + \gamma(TiAl) + \alpha_2(Ti_3Al).$$

In agreement with Pedrix et al.,[16] the increment in volume fraction of α_2 in the FGM composite clads with increased LED as seen in the XRD analysis suggests that increased carbon in the solid solution as LED increases leads to enhancement of the stability of the elevated temperature α phase. Furthermore, the Ti-Al-C phase diagram also confirms that the solubility of carbon in the α_2 phase is higher relative to that of the γ phase.[14] The increased metallurgical reaction among Ti, Al and C at the highest LED suggests that increased laser power enhances the available heat being dissipated to the powder blends.

Consequently, this raises the temperature of the melt pool as well as the propensity of the laser-materials interaction to form an intermetallic compound as an increasing amount of TiC dissolved into the melt pool. The precipitation of primary TiC from the melt upon solidification in all the samples could be attributed to the fact that the carbon content in the melt pool (Table Ia and b) is higher than 2 at.% irrespective of the LED adopted to fabricate the

FGM composite clads. However, the dissolved carbon content in the melt pool varies depending on the LED adopted for processing. Each of the FGM composite clads fabricated in this study consists of five different layers regarding the composition and structure of each layer. Therefore, the composition as well as microstructure of each layer is a function of the composition of the powder blends and LED. The dilution resulting from the melting of one layer upon the other as well as its solidification phenomenon is manipulated by the LED. It is expected that a minimum dilution between the first layer and substrate will be attained by selecting the appropriate LED parameter to impart the desirable composition. Further studies will explore the alteration in the composition across the five layers of the FGM composite clads with reference to the Ti-Al-C ternary system.

Finally, evidence from microstructural/microhardness studies, chemical composition and phase analysis of the samples indicates that reaction synthesis will not take place between Ti and Al when the LED < 17.50 J/mm^2. Therefore, the formation of intermetallic compounds (e.g. Ti_2AlC, γ and α_2 matrix phases) results from thermo-positive reactions between Ti-Al. Prior to the commencement of the reaction synthesis via LC processing, the powder blends (Fig. 7bi) were heated near or thereabout the melting of aluminium. Consequently, molten aluminium reacts with Ti particles via a thermo-positive reaction that produces a range of products including the following: $3Ti + Al \rightarrow Ti_3Al$; $Ti + Al \rightarrow TiAl$ (Fig. 7bii). As a result, the temperature of the whole system is deemed to rise abruptly and this induces a chain reaction in the entire system. With increasing LED, the temperature of the melt pool exceeds the melting point of Ti-Al and TiC. This eventually initiates a violently thermo-positive reaction thereby causing a metallurgical reaction leading to the formation of γ-TiAl, α_2-Ti_3Al and Ti_2AlC (Fig. 7biv).

CONCLUSION

1. Based on microstructural evidence obtained from this study, the particle size of unmelted titanium carbide diminished in varying degrees, depending on the applied LED, relative to the particle size of the starting powder, which lies between 45 μm and 90 μm. This suggests that TiC particles melted and dissolved in the melt pool.
2. The impartation of microhardness values higher than those of the substrate for the FGM composite clad fabricated with 17.50 J/mm^2 could be attributed to (1) the Ti-Al matrix alloying with aluminium as well as the partial melting of TiC, which results in the precipitation of primary TiC crystals, and (2) refinement of the microstructure at these layers upon the occurrence of the phenomenon of rapid solidification.
3. A variation in microhardness across the layers of the sample fabricated with LED of 17.50 J/mm^2 could be attributed to the influence of different laser-materials interactions accounted for by differing chemical compositions across the FGM volume. Therefore, the composition and microstructure of each layer of the FGM composite is not only a function of the composition of the powder blends but also that of the LED.
4. Crack frequency varies inversely to the LED. Consequently, a diminishing tendency of the occurrence of cracking at higher incident LED is accounted for by the resultant lower cooling rates.
5. The nature as well as mechanism of crack propagation in LC-fabricated Ti-Al FGM composite coating is a function of LED. At low LED, cracks originate from the boundary of unmelted TiC particles because of poor bonding between the unmelted Ti-C particle and solidified Ti-Al matrix, whereas stronger bonding exists between the partially melted Ti-C particle and solidified Ti-Al matrix when samples are fabricated with higher LED. Consequently, no crack is propagated from the boundary of partially melted TiC particles at higher LED.
6. During the LC processing of the FGM composite clads, it was discovered that when titanium diffuses faster, both aluminium and carbon tend to diffuse very slowly and vice versa. Moreover, titanium diffuses faster than both aluminium and carbon at higher LED.
7. When the LED was set at 12.50 J/mm^2 and 15.00 J/mm^2, the induced processing temperature associated with the synthesis reaction of the powder blends was just adequate to affect the melting of aluminium.
8. FGM composite clads were fabricated from Ti-Al blended with TiC when LED was set at 17.50 J/mm^2. At the selected LED, a thermo-positive reaction between the constituent materials was induced and resulted in the formation of intermetallic compounds (e.g. Ti_2AlC, γ and α_2 matrix phases).

ACKNOWLEDGEMENTS

This research was supported by the African Laser Center (ALC) under Grant No. CSIR-NLC (Reference LHIL 500 task ALC R008 & R010) and Botswana International University of Science and Technology (BIUST) Research Initiation Fund under Grant No. BIUST/ds/r&I/7/2016. Special thanks to the Office of the Deputy Vice-Chancellor Academic Affairs at BIUST for sponsoring the first author's attendance at the 2018 Solid Freeform Fabrication Forum at University of Texas, Austin, USA, August 2018. The technical support from Mr. G. Rabalone and Mr. Madiba towards sample characterisation is acknowledged while Mr. Thatayaone Lekang's assistance with Fig. 7b is appreciated.

REFERENCES

1. B. Cárcel, A. Serrano, J. Zambrano, V. Amigó, and A.C. Cárcel, *Phys. Procedia* 56, 284 (2014).
2. J.H. Abboud, D.R.F. West, and R.D. Rawlings, *J. Mater. Sci.* 29, 3393 (1994).
3. E.O. Olakanmi, S.T. Nyadongo, K. Malikongwa, S.A. Lawal, A. Botes, and S.L. Pityana, *Surf. Coat. Technol.* 357, 289 (2019). https://doi.org/10.1016/j.surfcoat.2018.09.063.
4. M.A. Zavareh, E. Doustmohammadi, A.A.D.M. Sarhan, R. Karimzadeh, P.M. Nia, and R.S.A. Singh, *Ceram. Int.* 44, 12180 (2018).
5. W. Li, S. Karnati, C. Kriewall, F. Liou, J. Newkirk, K.M.B. Taminger, and W.J. Seufzer, *Addit. Manuf.* 14, 95 (2017).
6. Y. Zhang, W. Ni, and Y. Li, *Ceram. Int.* 44, 11166 (2018).
7. A. Nazarov, V.A. Safronov, R.S. Khmrov, and I. Shishkovsky, *Procedia IUTAM* 23, 161 (2017).
8. S.E. Hoosain, S.L. Pityana, M. Tlotleng, and T. Legopeng, A comparative study on laser processing of commercially available titanium aluminide (TI-48AL-2CR-2NB) and in situ alloying of titanium aluminide, in *Presented at the 18th Annual International Rapid Product Development Association of South Africa (RAPDASA)*, 7–10 November 2017, Durban ICC, South Africa. https://researchspace.csir.co.za/dspace/bitstream/handle/10204/9805/Hoosain_19844_2017.pdf?sequence=1&isAllowed=y. Accessed on 1 June 2018.
9. B.N. Masina, T. Lengopeng, S.L. Pityana, and M. Tlotleng, *S. Afr. J. Ind. Eng.* 28, 172 (2017).
10. N. Mizuta, K. Matsuura, S. Kirihara, and Y. Miyamoto, *Mater. Sci. Eng. A* 492, 199 (2008).
11. I. Shishkovsky, F. Missemer, and I. Smurov, *Comput. Struct.* 83, 663 (2018).
12. S. Kou, *Welding Metallurgy* (New York: Wiley, 1987), p. 46.
13. R.A. Patterson, P.L. Martin, B.K. Damkroger, and L. Christodoulou, *Welding J.* 69, 39s (1990).
14. W. Liu and J.N. DuPoint, *Metall. Mater. Trans. A* 35A, 1133 (2004).
15. H. Chen, *Mater. Charact.* 136, 44 (2018).
16. F. Perdrix, M. Trichet, J. Bonnentien, M. Cornet, and J. Bigot, *Intermetallics* 9, 807 (2001).